Unstructured Unsteady Flow Solver Applicable to MSU TURBO and Computational Design

Final Report for NASA Glenn Grant NAG3-2829

for

Dr. Eric McFarland
NASA Glenn Research Center
Mail Stop 5-10
21000 Brookpark Road
Cleveland, Ohio 44135

by

James C. Newman III and Chunhua Sheng

Computational Simulation and Design Center
February 2004

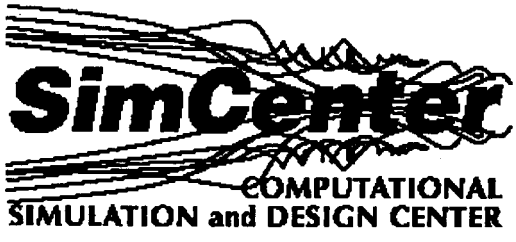

Mississippi State University
P.O. Box 9627
Mississippi State, MS 39762

NASA Glenn Research Center Grant NAG3-2829

Unstructured Unsteady Flow Solver Applicable to MSU TURBO and Computational Design

James C. Newman III and Chunhua Sheng

Summary Research Report for Budget Period

This final report is divided into two sections: **I.** research performed to advance the analysis capabilities of the U^2NCLE software for turbomachinery applications, and **II.** research performed to enhance this software with sensitivity analysis capabilities.

Section I

Advances in the Analysis Capabilities of the U^2NCLE Software for Turbomachinery Applications

42nd AIAA Aerospace Sciences Meeting and Exhibit AIAA-2004-372
Reno, Nevada, 5-9 January 2004

Numerical Simulations of Rotor 35 With and Without Tip Injection Using an Arbitrary Mach Number Flow Solver

Chunhua Sheng* **and Michael Remotigue†**

Computational Simulation and Design Center
Mississippi State University, MS 39762, USA

Abstract

This paper presents numerical simulations for a high–speed transonic compressor rotor, NASA Rotor 35, using an unstructured grid flow solver U²NCLE. It solves Reynolds averaged Naiver–Stokes equations using an arbitrary Mach number solution algorithm. Experiments were conducted at the NASA Gleen Research Center to investigate compressor stability enhancement using steady and discrete tip injections. The mass injection upstream of the tip of a high–speed axial compressor rotor has shown effectiveness in suppressing stall in tip–critical rotors. This work presents numerical simulations of a high–speed compressor rotor with and without tip injections. Methods to model the flow injection are described. Numerical simulations are conducted at 80 and 100 percent of the design speed. Results show that numerical solutions are consistent with the experimental trends.

Introduction

A research effort supported by the NASA Glenn Research Center was initiated in 2001 for the purpose of exploring the use of an unstructured solver in the calculation of turbomachinery flows, and specifically, to consider the possible benefits of developing an unstructured version of the MSU TURBO code [1]. Whereas the present MSU TURBO code, distributed to U.S. engine companies by NASA Glenn, is a heavily used parallel unsteady compressible Reynolds averaged Navier–Stokes flow solver, it is a multiblock code that uses structured subgrids. Consequently, there are some geometric configurations that are difficult and time consuming to grid. For example, the Army Research Laboratories Vehicle Technology Directorate (VTD) has an urgent need for the capability to numerically simulate the flow through centrifugal compressors with vaned diffusers, which are difficult to grid using structured grid technology due to the complexity of the geometry. In the past few years an unstructured Reynolds averaged Navier–Stokes flow solver, referred to as U²NCLE (Unstructured UNsteady Computation of fieLd Equations), has been developed in the Computational Simulation and Design Center at Mississippi State University for compressible, incompressible, and arbitrary Mach number flow regions [2–4]. It is prudent to consider the use of this new technology for application to turbomachinery.

The test case studied in this work is a high–speed axial compressor rotor, NASA Rotor 35. Experiments to enhance the stability of an axial compressor rotor using tip injection techniques were conducted by Suder, et al. [5] at the NASA Glenn Research Center. They found that mass injection upstream of the tip of a compressor rotor was effective in suppressing stall in tip–critical rotors. Experiments also showed that stability enhancement was related to the mass–averaged axial velocity at the tip, and the configuration of the injector. To investigate the impact of injector parameters on stability improvement for an axial compressor rotor, Suder, et al. [5] performed numerical simulations using the Average Passage code (APNASA) developed by Adamczyk [6]. Time–accurate unsteady simulations for a transonic compressor stage, Stage 35, with tip injections were recently conducted at the Computational Simulation and Design Center at Mississippi State University using the MSU–TURBO code [7]. These investigations indicate that the effect of the injection is sensitive to the momentum and velocity of the flow leaving the injector. The injector effectiveness is maximized when the injected flow is choked.

The purpose of this work is to assess the capability and accuracy of the current unstructured grid flow solver U²NCLE to compute flows in turbomachinery. It is intended to develop a methodology to simulate flow injections and analyze the effect of stability enhancement on high–speed compressor rotors and stages. The technology developed in this work will later be used to investigate the stall inception process and stall control techniques in a high–speed centrifugal compressor stage being tested at the US Army Research Laboratory. To this end, two computational meshes are generated for

*Associate Research Professor, Member AIAA
†Assistant Research Professor

simulations of an isolated Rotor 35 with and without tip injections. There are 12 injectors uniformly spaced around the compressor annulus upstream of the rotor tip in the experiment. However, this work solves only one injector and three blade passages based on the periodicity of the flow field. Numerical simulations are conducted at 80 and 100 percent of the design speed. All computational results, including with and without injection flows, are verified with the experimental data.

Numerical Methods

To simulate complex viscous flows in turbomachinery, a parallel version of an unstructured Reynolds averaged Navier–Stokes flow solver U²NCLE was developed at the Computational Simulation and Design Center at Mississippi State University [4]. The solver solves preconditioned three–dimensional compressible governing equations in absolute reference frame and/or rotating reference frame. The numerical scheme, referred to as an arbitrary Mach number solution algorithm [8], allows calculations of both low–speed and high–speed flows in turbomachinery. Validation and verification of the U²NCLE solver for isolated rotors for low Mach number and transonic flows have been reported in [4][9].

Primitive–Variables Conservation Laws

The unsteady three–dimensional compressible Reynolds–averaged Navier–Stokes equations are cast in a rotating Cartesian coordinate system with a rotational speed of Ω. The conservative flux formulation is written in terms of primitive variables in the absolute frame. In order to solve arbitrary Mach number flows, a preconditioning matrix Γ_q^{-1} is introduced into the primitive variable conservation laws, which can be expressed as

$$M\Gamma_q^{-1}\frac{\partial}{\partial t}\int_{\Omega} q\,dV + \oint_{\partial\Omega} \boldsymbol{F}\cdot\hat{n}\,dA = \int_{\Omega} S\,dV \quad (1)$$

where Γ_q^{-1} is a constant diagonal matrix that only depends on the reference Mach number M_r [8][10]

$$\Gamma_q^{-1} = diag\left[1, 1, 1, 1, 1/\beta(M_r)\right] \quad (2)$$

and M is a transformation matrix from conservative variables $\boldsymbol{Q} = (\rho, \rho u, \rho v, \rho w, \rho e_t)^T$ to primitive variables $q = (\rho, u, v, w, p)^T$, where u, v, and w, are the absolute velocity components in x, y, and z directions, respectively. ρ is the density; p is the pressure; and e_t is the total energy. $\hat{n} = (n_x, n_y, n_z)^T$ is the outward pointing unit normal to the surface of the control volume dV. $\boldsymbol{F}$ is vectors of both inviscid and viscous fluxes, which is given as

$$\boldsymbol{F}.\hat{n} = \begin{bmatrix} \rho\Theta \\ \rho u\Theta + n_x p - T_x \\ \rho v\Theta + n_y p - T_y \\ \rho w\Theta + n_z p - T_z \\ \rho h_t\Theta - n_t E_c p - uT_x - vT_y - wT_z + Q_n \end{bmatrix} \quad (3)$$

where $E_c = (\gamma - 1)M_r^2$ is an Eckardt number. Θ is the normal velocity with respect to the surface of a control volume. The viscous shear stresses are given as

$$T_x = n_x\tau_{xx} + n_y\tau_{xy} + n_z\tau_{xz}$$
$$T_y = n_x\tau_{yx} + n_y\tau_{yy} + n_z\tau_{yz}$$
$$T_z = n_x\tau_{zx} + n_y\tau_{zy} + n_z\tau_{zz}$$

where

$$\tau_{xx} = \frac{\mu}{\mathrm{Re}}\frac{2}{3}\left(2\frac{\partial u}{\partial x} - \frac{\partial v}{\partial y} - \frac{\partial w}{\partial z}\right)$$
$$\tau_{yy} = \frac{\mu}{\mathrm{Re}}\frac{2}{3}\left(2\frac{\partial v}{\partial y} - \frac{\partial u}{\partial x} - \frac{\partial w}{\partial z}\right)$$
$$\tau_{zz} = \frac{\mu}{\mathrm{Re}}\frac{2}{3}\left(2\frac{\partial w}{\partial z} - \frac{\partial u}{\partial x} - \frac{\partial v}{\partial y}\right)$$
$$\tau_{xy} = \tau_{yx} = \frac{\mu}{\mathrm{Re}}\left(\frac{\partial u}{\partial y} + \frac{\partial v}{\partial x}\right)$$
$$\tau_{xz} = \tau_{zx} = \frac{\mu}{\mathrm{Re}}\left(\frac{\partial u}{\partial z} + \frac{\partial w}{\partial x}\right)$$
$$\tau_{yz} = \tau_{zy} = \frac{\mu}{\mathrm{Re}}\left(\frac{\partial v}{\partial z} + \frac{\partial w}{\partial y}\right)$$

S is the source term representing both body forces S_{bf} in rotating coordinates, as well as injected flows S_{inj}, which will be described next.

Note that the above equations are non–dimensionalized by the following reference values: density, ρ_r; velocity, U_r; temperature, T_r, pressure, $\rho_r U_r^2$; length, L_r; time, L_r/U_r; energy and enthalpy, C_pT_r.

Source Term

The source term in the above Eq. (1) has two parts

$$S = S_{bf} + S_{inj}$$

$$S_{bf} = \begin{bmatrix} 0 \\ \rho w\Omega_y - \rho v\Omega_z \\ \rho u\Omega_z - \rho w\Omega_x \\ \rho v\Omega_x - \rho u\Omega_y \\ 0 \end{bmatrix} \quad S_{inj} = \frac{1}{\forall}\begin{bmatrix} \dot{m}_{inj} \\ \dot{m}_{inj}u_{inj} \\ \dot{m}_{inj}v_{inj} \\ \dot{m}_{inj}w_{inj} \\ \dot{m}_{inj}e_{inj} \end{bmatrix} \quad (4)$$

where S_{bf} is the body force (Coriolis and centrifugal forces) in rotating coordinates, and Ω_x, Ω_y, and Ω_z are the components of the rotational speed Ω of the coordinate system. The second term S_{inj} is used to model the effect

of injected flows by adding the extra mass, momentum, and energy into the governing equations. $\dot{m}_{inj}$ is the injected massflow rate, $u_{inj}, v_{inj}, w_{inj}$ are the injected velocity components in x, y, z directions, and e_{inj} is the total energy of injected flow. $\forall$ is the total volume of cells that injected flow is added on. An uniform velocity distribution is assumed on the injector area. Noting that S_{bf} is added to all control volumes in rotating coordinates, while S_{inj} is only added to regions that are marked as the injector area.

Numerical Schemes

Preconditioned equations (1) can be expressed in a differential form as

$$M\Gamma_q^{-1}\frac{\partial q}{\partial t} + M\Gamma_q^{-1}|\Gamma_q M^{-1}AM|\frac{\partial q}{\partial x} = S \qquad (5)$$

where $\Gamma_q M^{-1}AM$ is the system matrix for preconditioned equations, and $A = \partial F/\partial Q$ is the flux Jacobian with respect to Q. The inviscid flux approximation at the face of a control volume for the preconditioned system is

$$F_i = \frac{1}{2}(F(q_L) + F(q_R)) - \frac{1}{2}\hat{M}\Gamma_q^{-1}|\Gamma_q \hat{M}^{-1}\hat{A}\hat{M}|(q_R - q_L) \qquad (6)$$

The eigensystem of the above Eq. (6) is evaluated based on the averaged variables $\hat{q}$.

$$\begin{aligned}\hat{\rho} &= \frac{1}{2}(\rho_L + \rho_R)\\ \hat{u} &= \frac{1}{2}(u_L + u_R)\\ \hat{v} &= \frac{1}{2}(v_L + v_R)\\ \hat{w} &= \frac{1}{2}(w_L + w_R)\\ \hat{h}_t &= \frac{1}{2}(h_{t_L} + h_{t_R})\end{aligned} \qquad (7)$$

Since the eigensystem and the flux are evaluated based on the above averaged variables instead of Roe variables, the current approach is considered to be an extension of the Roe flux approximation [10]. For first–order accurate differencing, quantities q_L and q_R are set equal to the data at the nodes lying on either side of the face. For a second–order scheme, these values are computed with a Taylor series expansion about the central node of the control volume with an unweighted least–squares procedure [11].

There are two issues in reconstructing the viscous scheme. One is the positivity of the discrete operator, which requires that all of the stencil weights be positive. Positivity is a key property for numerical stability. Another key property is the linearity–preserving of gradients, which means that for a linear distribution of velocity, one should obtain a constant gradients of velocity. In this work, a positive scheme proposed in [8] is used to compute gradients of flow variables at the medial dual faces for stable and accurate simulations of viscous flows.

The numerical algorithm is based on a node–centered, finite volume implicit scheme on unstructured mixed element grids. The time–advancement algorithm is based on Newton's method, which yields a linear system of equations for the solution at each time step. The solution of the sparse system of equations is obtained by symmetric Gauss–Seidel relaxations. Normally 8~15 symmetric Gauss–Seidel subiterations are adequate at each time step.

Turbulence Model

The current U²NCLE solver has several turbulence model options, including Spalart and Allmaras one–equation model [12], and q–ω, k–ε, k–ω two–equation models [13]. These turbulence models are loosely coupled with the mean flow equations, meaning that they are solved separately following the mean flow solution at each time step. This has an advantage of easily modifying the existing models or adding a new turbulence model to the solver. For the current study, one–equation turbulence model of Spalart and Allmaras is used in all calculations. Since there is no wall–function model used in the solver, grid points need to be packed near viscous surfaces in order to fully resolve the boundary layer. An ongoing effort is to explore the use of two–equation models for future turbomachinery simulations.

It should be noticed that a source term for the eddy viscosity is added to the Spalart and Allmaras turbulence equation to model the flow injection. This is necessary to maintain a stable solution for the strong mixing between the injected flow and the primary flow. The amount being added to the turbulence equation is estimated based on the injected massflow rate in the current work, although a more accurate value may be obtained from the measured data.

Boundary Conditions

The boundary conditions required for turbomachinery flow computations were derived in detail in Ref. [9]. These boundary conditions are based on characteristic relations that propagate in the direction of characteristic waves, i.e. the eigenvalues of preconditioned system of equations. Under the current grid topology, all boundary faces have positive outward pointing normals. A positive eigenvalue means that the corresponding char-

acteristic wave propagates from the interior domain to the boundary, while a negative eigenvalue means that the characteristic wave propagates from the outside of the computational domain into the boundary. Those characteristic variables with negative eigenvalues are replaced by the total pressure and total temperature at the inflow, and the static pressure or radial equilibrium equation at the outflow for turbomachinery flow computations. The current unstructured flow solver has the following boundary conditions related to turbomachinery simulations:

- Inlet specifying total pressure, total temperature, and flow direction.
- Exit specifying constant back pressure.
- Exit with radial equilibrium condition.
- No–slip adiabatic wall.
- No–slip constant temperature wall.
- Rotating viscous surface for shroud or hub.
- Periodical condition for axisymmetry surfaces (require axisymmetry surface grids).
- Sliding interface for rotor/stator interaction.
- Source term for modeling injected flows.

Results

The test case studied in this work is a high–speed transonic compressor rotor, NASA Rotor 35. It has 36 blades, an inlet tip radius of 25.4 cm, a hub–tip radius ratio of 0.7, and aspect ratio of 1.19, a tip solidity of 1.3, and an axial chord of 2.72 cm at the tip and 4.12 cm at the hub. The compressor was designed for axial inlet flow, and inlet relative Mach number is 1.48 at the tip at the design speed. The rotor tip clearance at design speed is 0.86 percent of the tip chord. The compressor aerodynamic design and blade coordinates were reported by Reid and Moore [14].

Computations were performed at 80 and 100 percent of the design speed. The reference values at the inlet of the rotor are used to normalize the flow variables in the code. The reference Mach number is 0.52. The reference length is the rotor diameter. The Reynolds number is $5.2434 \times 10^{+6}$ based on the entrance velocity and the rotor diameter. Standard day pressure and temperature are used as the total conditions to specify the inflow boundary condition. Various back pressures are applied at the exit to obtain different operating conditions. All computations were carried out in parallel mode using Message Passing Interface (MPI) for interprocess communication. Simulations were performed on a large–scale Linux cluster (1024 Intel Pentium III 1.3 GHz processors and 512 MB RAM per processor) located at the Engineering Research Center at Mississippi State University.

Rotor 35 without Tip Injection

The first case studied is an isolated rotor without tip injection. Simulations were conducted to obtain the baseline operating characteristics at 80 percent of the design speed (a peak efficiency operating condition). This corresponds to a speed of 13,755 rev/min and a rotor tip speed of 363 m/s. Laser Doppler Velocimeter (LDV) measurements [15] were acquired in the NASA Glenn single–stage axial flow compressor facility using the NASA Rotor 35 operating in a rotor–only configuration, and are used to verify the computed results. The computational grid (Figure 1) was generated for a single blade passage using a grid generation tool GUM–B [16]. A periodical boundary condition is applied at the axisymmetric surfaces. In order to simulate the tip clearance flow, a true gap was generated between the rotor tip and the casing, see Figure 2. The grid has approximately one million points, which is partitioned into 32 block for parallel computations. Simulations were conducted in the rotating reference frame by solving absolute velocity components. Solutions were considered converged when the difference between the inlet and the exit massflows was below one percent of the total massflow.

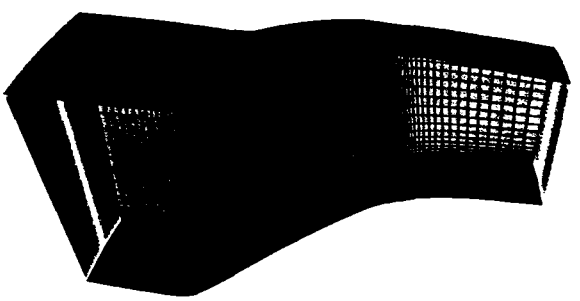

Figure 1 Single Passage Grid for Rotor 35

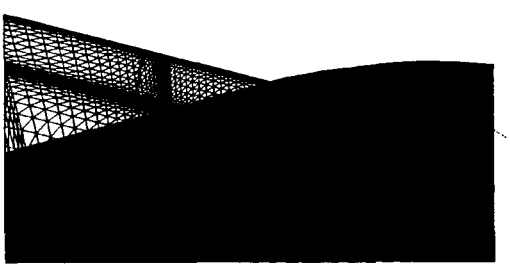

Figure 2 Cutting Plane Grid in Tip Clearance

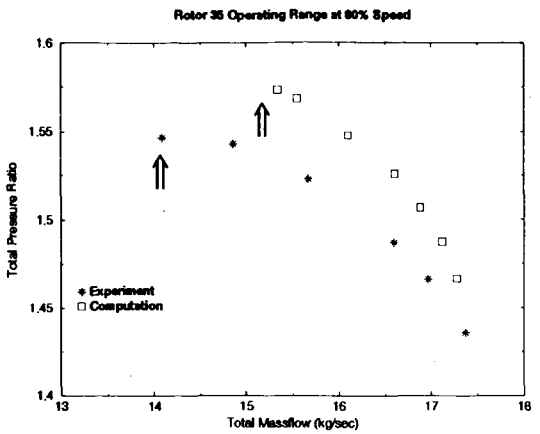

Figure 3 Computed and Measured Rotor 35 Operating Range at 80% of Design Speed

Figure 3 shows the comparison of measured and computed total pressure ratios for Rotor 35 at 80 percent of the design speed. The computed operating curve was obtained by gradually increasing the back pressure at the exit in the computational domain, starting from a value of 96,818 N/m^2 (Pa) on the shroud. The measured total pressure ratio and efficiency at peak operating condition are 1.44 and 92 percent respectively, which corresponds to a massflow of 17.35 kg/s. The computed total pressure ratio and efficiency which are closest to the experimental data are 1.46 and 90.4 percent, respectively. The computed and measured stall points are marked with arrows in Figure 3. It seems that computations overpredicted the total pressure ratio at the near stall point by 3 percent. The predicted stable operating range is smaller than the measured value (the computed stall massflow is larger than the experimental data), which could be caused by the grid resolution and the tip treatment. Van Zante, et al. [15] studied three different tip grid topologies and their impact on the predicted stability. They found that the trajectory of the clearance vortex can be influenced by different tip grid treatments, which in turn affect the stability of the rotor. However, the study on grid resolutions was not conducted in the current work, and will be conducted in the future. Nevertheless, the above computed operating characteristic curve matches with the experimental trend.

The tip clearance vortex has a great impact on the rotor performance. Hoying, et al. [17] and Adamczyk, et al. [18] suggest that rotor stall occurs when the tip clearance vortex spills forward of the leading edge. It is very important that the tip vortex and its trajectory are

Experiment Computation

Figure 4 Computed and Measured Axial Velocity (m/s) on the 92% Span Stream Surface at Near Peak Efficiency

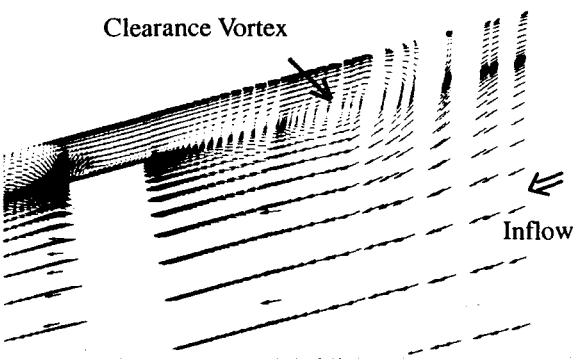

Figure 5 Velocity Vectors on x–r Cutting Plane

correctly predicted in the numerical simulations. Figure 4 shows computed contours for axial velocity for the 92 percent span stream surface, and measured contours by Van Zante, et al. [15]. These plots clearly illustrate the lower extent of the flow field region impacted by the tip clearance flow. The axial velocity is chosen here since the footprint of the clearance flow shows most clearly as gradients in axial velocity on this stream surface. Figure 5 shows computed velocity vector on

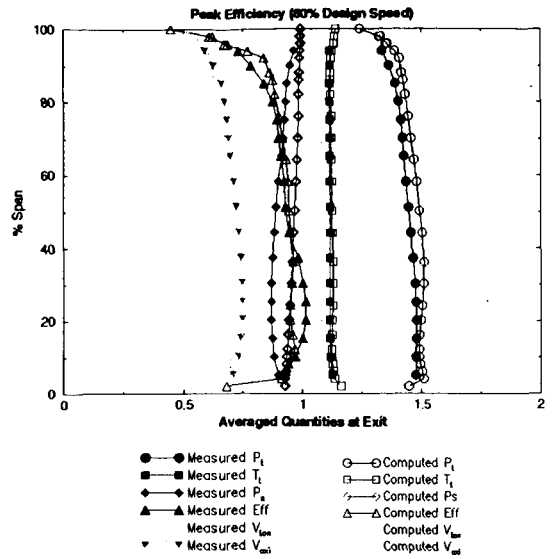

Figure 6 Computed and Measured Exit Variables at Peak Efficiency

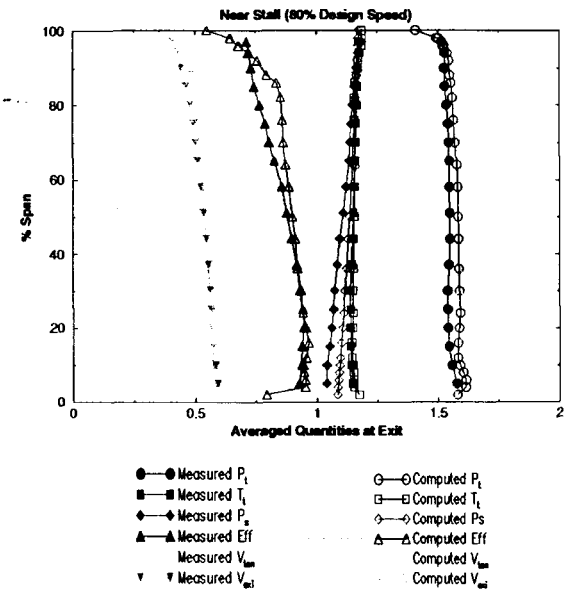

Figure 7 Computed and Measured Exit Variables at Near Stall Point

the x–r cutting plane at the middle chord location, with the axial flow coming from the right. A tip vortex is clearly observed in the numerical solution. The trajectory of the clearance vortex is determined by the wall-bounded shear layer near the shroud. The computed clearance vortex matches with the numerical results obtained by Van Zante, et al. [15]. However, an induced vortex captured in Ref. [15] is not observed here, which may be due to the lack of grid resolution in the region. Van Zante, et al. [15] suggested that the induced vortex has a strong impact on the rotor stability. The rotor stability can be enhanced by increasing the strength of the induced vortex. It is believed that a refined grid in the tip region may help capture the induced vortex, and thus improve the predicted operating characteristics as well.

Figures 6 and 7 show comparison of computed and measured total pressure P_t, total temperature T_t, static pressure p_s, adiabatic efficiency η, absolute tangential velocity V_t, and axial velocity V_x at the exit of the blade passage along the spanwise direction. These quantities are obtained by a massflow averaging procedure along the circumferential direction at each span location. Comparisons are made at the peak efficiency and the near stall point. Computed total pressures (and static pressures) at both operating points overpredict the measured values, which is consistent with predicted results shown in Figure 3. The overpredicted pressure leads to slight deviation of adiabatic efficiency. However, computed results in general match well with the experimental data.

Rotor 35 with Tip Injection

As mentioned in the introduction, one goal of this work is to develop a methodology to simulate flow injections in high–speed transonic compressors, and to investigate the stabilizing effect of tip injections on compressor performance. Casing–mounted injectors are located 55 cm (about 200 percent of rotor tip axial chord) upstream of the rotor. There are 12 injectors uniformly spaced around the compressor annulus, which are designed to generate a jet along the casing upstream of the rotor. Both numerical simulations and experimental measurements were conducted by Suder, et al. [5] to investigate the compressor stability enhancement using the tip injection. The impact of tip injection on the stability limit of an axial compressor stage was investigated by Weigl, et al. [19]. Their studies showed that jet flows upstream of the rotor tip were effective in suppressing the stall inception in the axial compressor rotor and stage. The measured extension of operating range for an isolated rotor was about 30 percent at 70 percent of the design speed. The extension of operating range at 100 percent of the design speed was less than what was achieved at 70 percent of the design speed, but was still noticeable. Figure 8 shows impact of the tip injection on the stability limit for a transonic axial compressor stage as measured by Weigl et al. [19].

The current work simulates a steady tip injection upstream of an isolated Rotor 35 at the design speed, using an unstructured grid flow solver. The standard day

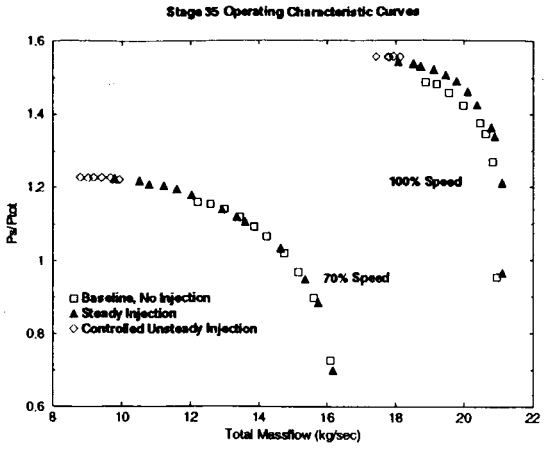

Figure 8 Impact of Tip Injection on the Stability Limit of a Transonic Axial Compressor Stage Measured by Weigl, et al. [19]

corrected speed for the design flow condition is 17,188.7 rev/min with a rotor tip speed of 454.14 m/s. The effective injector size in the grid is 4.73 mm in depth and 40.23 mm in width, which covers about 75 percent of the actual injector exit area. An uniform velocity across the injector exit is assumed. The injected flow is aligned with the inlet annulus flow in the downstream axial direction to minimize mixing between the annulus flow and the injected flow. The stagnation pressure for the injected flow is 1.88 times the standard day pressure, and the stagnation temperature of the injected flow is the same as the standard day temperature. A choke flow is assumed at the injector exit, which results in a mass flow of 1.026 kg/s (about 5 percent of rotor choke flow). Figure 9 shows the computational mesh which includes one injector and three rotor–blade passages in a 30–degree segment. There is an interface between the injector and the rotor which divides the computational mesh into two components, the injector grid and the rotor grid. The grid points are smoothly connected between the injector and the rotor. Simulations are implemented in a steady–state mode, in which the flow in the injector grid is solved in the fixed absolute frame, while the flow in the rotor grid is solved in the rotating frame. Since the absolute velocity components are cast in the governing equations in both absolute and rotating frames, fluxes at the interface of the injector and the rotor are directly computed. Periodical boundary conditions are assumed at axisymmetric surfaces for both injector and rotor grids. Because there is no relative motion between the injector and the rotor, the above implementation can be viewed as to solve an isolated axial rotor with a stationary inflow source (injector) upstream of the rotor in rotating frame. This is an approximation to the physical problem in which the injector flow upstream of the rotor is actually rotating with respective to the rotor in rotating frame. The correct modeling of the physical problem would require unsteady time–accurate simulations using a sliding interface to account for the interaction between the injector and rotor, or solve an isolated rotor with an unsteady inflow boundary condition. The purpose of this work is to verify the unstructured flow solver to model flow injections with the source term method, and to predict (or estimate) the impact of tip injections on the rotor performance, rather than to provide a detailed analysis of the unsteady interaction between the injector and the rotor. The computational mesh has about three million points for both injector and rotor, and is partitioned into 96 blocks for parallel computations.

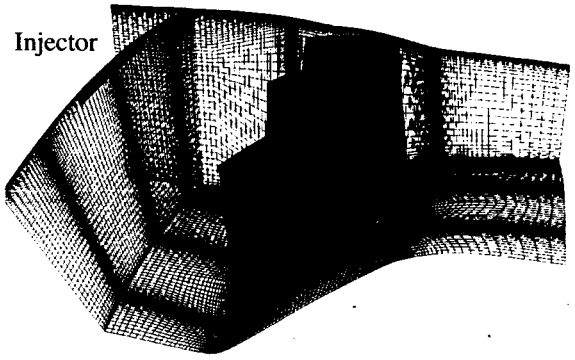

Figure 9 Three Blade Passage Grid for Rotor 35 with Tip Injector

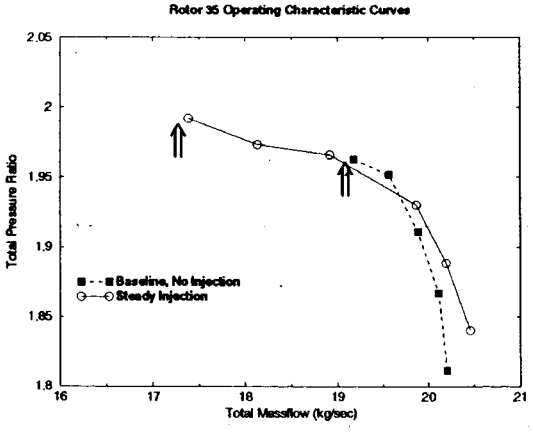

Figure 10 Predicted Rotor 35 Operating Ranges at 100% Design Speed

Figure 10 shows the predicted rotor performance at the design speed with and without the tip injection. The total massflow shown in Figure 10 is the sum of the inlet

corrected massflow and the injector corrected massflow, which is calculated based on the following formula

$$\dot{m}_{total} = \dot{m}_{inlet}\frac{\sqrt{T_{inlet}/T_{standard}}}{P_{inlet}/P_{standard}} + \dot{m}_{injector}\frac{\sqrt{T_{injector}/T_{standard}}}{P_{injector}/P_{standard}} \quad (8)$$

where T is the total temperature and P is the total pressure. Computed choke massflows with and without tip injection seem to be smaller than the measured values. The reason for this may be due to the pressure loss cased by the extended shroud and hub surfaces upstream of the rotor. The total pressure and the total temperature need to be adjusted at the inlet to match the correct state for the measurement. Computed baseline stall massflow (no injection) is 19.18 kg/s. Computed stall massflow with the flow injection is extended to 17.38 kg/sec. The stall back pressure (on shroud) is increased from 133,850 Pa in the case of no injection to 138,676 Pa in the case with injection. The stabilizing effect of the tip injection on rotor performance is clearly demonstrated. The predicted extension of operating ranges for Rotor 35 is very similar to the numerical results by Suder, et al. [5] using the APNASA code, and also matches with the experimental trend. It is noticed that no total pressure loss occurred when the flow was injected through the casing in the axial compressor rotor. This is different from what was observed in the experiment for a high-speed centrifugal compressor, where a total pressure loss occurred when the flow was injected in the diffuser [20].

Figures 11 and 12 show predicted static pressure and axial velocity contours with tip injection at a location of 98 percent span of the rotor. The interaction between the injected flow and the primary flow is clearly observed. The dash line indicates the interface between the injector grid and the rotor grid. It should be noticed that the flow field before the interface is viewed in the fixed frame, and the flow field after the interface is viewed in the rotating frame. The injected flow is pointed to the blade passage direction, rather than to the axial direction when it is viewed in the rotating frame. The effect of tip injections in suppressing the stall inception in the rotor is illustrated in Figure 13. The predicted axial velocity contours with and without tip injections at the same back pressure (133,850 Pa on the shroud) are shown in Figure 13 (a) and (b). Low velocity region occupied almost half of the blade passage at this back pressure in the case without tip injection, which led to continuous reduction of the massflow, and

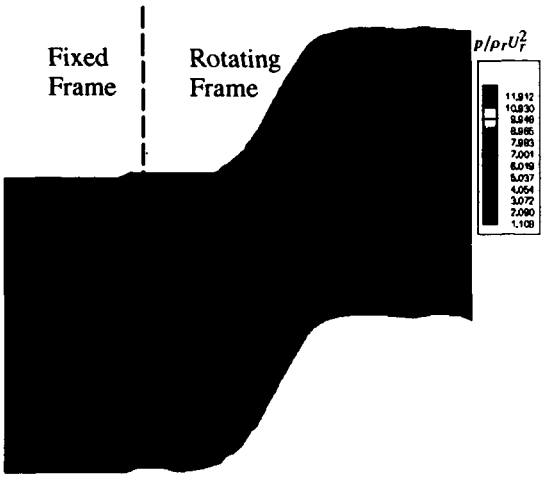

Figure 11 Static Pressure Contours at 98% Span of Rotor

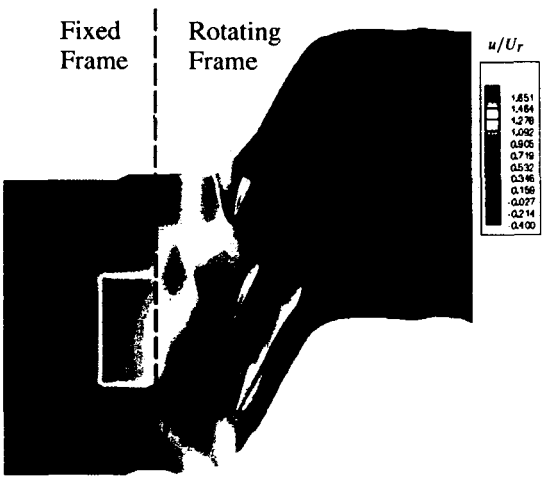

Figure 12 Axial Velocity Contours at 98% Span of Rotor

eventually to the stall condition. The flow field was well retained as the flow was injected upstream of the rotor, which increased the momentum of flows in the tip clearance region. A stable flow condition was maintained even at a higher back pressure, and the stall point was effectively extended.

As mentioned before, the current simulations only provide an estimate of the impact of tip injections on the performance of an axial compressor rotor. It is believed that the unsteady effect between the injector and rotor plays certain role in the stall inception process. Further more, because stall cells could rotate around the annulus of the compressor in the stall inception process which invalids the assumption of spacial and temporal periodicity, the correct way to model the stall inception process requires full annulus simulations of the compressor system. However, the current work demonstrated the

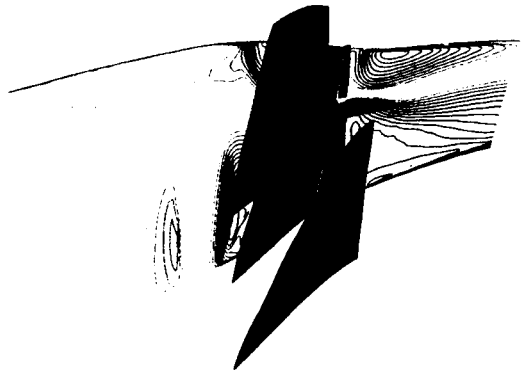

(a) Axial Velocity Contours Without Tip Injection

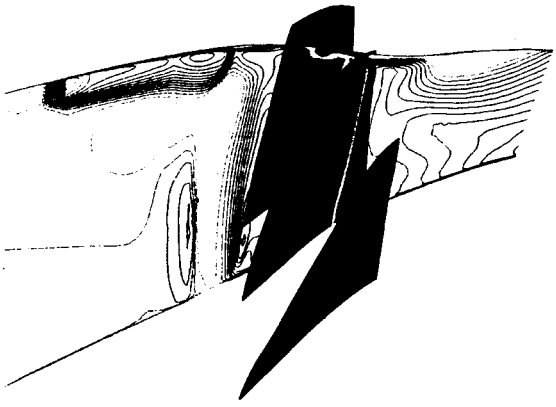

(b) Axial Velocity Contours With Tip Injection

Figure 13 Axial Velocity Contours on Cutting Plane Through Rotor Passage at a Back Pressure of 133,850 Pa

capability of the unstructured grid flow solver to simulate the flow injection in a high–speed axial compressor rotor, which is useful for future investigations on stall inception process and stall control techniques for a full annulus simulations of compressor systems.

Conclusions

Numerical methods to model tip injection flows in an isolated compressor rotor were presented based on a Reynolds averaged Navier–Stokes arbitrary Mach number flow solver. Simulations for a high–speed transonic compressor rotor, NASA Rotor 35 with and without tip injections were assessed with the experimental data. Computed operating ranges of Rotor 35 at 80 and 100 percent of the design speed matched with the experimental trend. The stability enhancement of tip injections on the rotor performance was demonstrated in the current work. Although the correct modeling of stall inception process requires time–accurate full annulus simulations of the compressor system, the methodology and numerical solutions presented in this work can be instructive for future investigations and optimizations of stall control techniques in gas turbine compressor systems.

Acknowledgement

This research was supported by the Army Research Office and NASA Glenn Research Center, with Drs. Michael Hathaway and Eric McFarland as technical monitors. These supports are gratefully acknowledged.

References

[1] Chen, J.P., "Unsteady Three–Dimensional Thin–Layer Navier–Stokes Solutions for Turbomachinery in Transonic Flow," Ph.D. Dissertation, Mississippi State University, December 1991.

[2] Hyams, D.G., Sreenivas, K., Sheng, C., Briley, W.R., Marcum, D.L., and Whitfield, D.L., "An Investigation of Parallel Implicit Solution Algorithms for Incompressible Flows on Multielement Unstructured Topologies," Proc., 38th Aerospace Sciences Meeting & Exhibit, AIAA Paper No. 2000–0271, Reno, NV, January 2000.

[3] Sheng, C., Hyams, D., Sreenivas, K., Gaither, A., Marcum, D.L., and Whitfield, D.L., "Three–Dimensional Incompressible Navier–Stokes Flow Computations About Complete Configurations Using a Multiblock Unstructured Grid Approach," 37th AIAA Aerospace Science Meeting and Exhibit, January 11–14, 1999, Reno, NV.

[4] Sheng, C., Newman III, J., Remotigue, M., Chen, J.P., Marcum, D., and Whitfield, D., "Development of Unstructured Computational Capabilities Applicable to MSU TURBO with an Arbitrary Mach Number Algorithm," MSSU–COE–ERC–02–16, Mississippi State University, October 2002.

[5] Suder, K. L., Hathaway, M. D., Thorp, S. A., Strazisar, A. J., and Bright, M., B., "Compressor Stability Enhancement Using Discrete Tip Injection," Proceedings ASME TURBO EXPO 2000, International Gas Turbine and Aeroengine Comgress, May 8–11, 2000, Munich, GERMANY

[6] Adamczyk, J.J., "Model Equation for Simulating Flows in Multistage Turbomachinery," ASME Paper No. 85–GT–226, 1985.

[7] Hathaway, M.D., Chen, J.P., and Webster, R.S., "Time Accurate Unsteady Simulation of Stall Inception Process in the Compression System of a US Army Helicopter Gas Turbine Engine," DoD HPCMP User's Group Conference (UGC), Bellevuew, Washington, June 9–13, 2003.

[8] Sheng, C., Taylor, L.K., Briley, W.R., and Whitfield, D.L., "An Unstructured Arbitrary Mach Number Algorithm for Viscous Flows in Turbomachinery," to appear in Computers & Fluids, October 2003.

[9] Sheng, C., Wang, X., "Characteristic Variable Boundary Conditions for Arbitrary Mach Number Algorithm in Rotating Frame," AIAA Paper 2003–3976, 16th AIAA Computational Fluid Dynamics Conference, June 23–26 2003, Orlando, FL.

[10] Briley, W.R., Tayler, L.K., and Whitfield, D.L., "High–Resolution Viscous Flow Simulations at Arbitrary Mach Number," *Journal of Computational Physics*, 184(1), 79–105, 2003.

[11] Anderson, W.K., Rausch, R.D., and Bonhaus, D. L., "Implicit/Multigrid Algorithms for Incompressible Turbulent Flows on Unstructured Grids," AIAA Paper 95–1740, June 1995.

[12] Spalart P., and Allmaras, S., "A One–Equation Turbulence Model for Aerodynamic Flows," AIAA Paper 92–0439, January 1991.

[13] Shringi, V., "Implementation of Two–Equation Turbulence Models in U2NCLE," MS Thesis, College of Engineering, Mississippi State University, 2001.

[14] Reid, L. and Moore, R.D., "Performance of Single–Stage Axial–Flow Transonic Compressor with Rotor and Stator Aspect Radios of 1.19 and 1.26, respectively, and with Design Pressure Radio of 1.82," NASA TP 1338, 1978.

[15] Van Zante, D.E., Strazisar, A.J., Wood, J.R., Hathaway, M.D., and Okiishi, T.H., "Recommendations for Achieving Accurate Numerical Simulation of Tip Clearance Flows in Transonic Compressor Rotors," *NASA TM–2000–210347*, NASA Glenn Research Center, September 2000.

[16] Remotigue, M.G., "A Pre–Processing System for Structured Multi–Block Parallel Computations", Numerical Grid Generation in ComputationalField Simulations. Proceedings of the 8th International Conference, Honolulu, Hawaii, June 2002.

[17] Hoying, D.A., Tan, C.S., Vo, H.D., and Greitzer, E.M., "Role of Blade Passage Flow Structures in Axial Compressor Rotating Stall Inception," ASME Paper No. 98–GT–588, 1998.

[18] Adamczyk, J.J., Celestina, M.L., and Greitzer, E.M., "The Role of Tip Clearance in High–Speed Fan Stall," ASME Journal of Turbomachinery, Vol. 115, pp. 28–38, 1993.

[19] Weigl, H.J., Paduano, J.D., Frechette, L.G., Epstein, A.H., Greitzer, E. M., Bright, M.M., and Strazisar, A.J., "Active Stabilization of Rotating Stall and Surge in a Transonic Single Stage Axial Compressor," ASME Journal of Turbomachinery, Vol. 120, No. 4, pp. 625–636.

[20] Skoch, G.J.,"Emperimental Investigation of Centrifugal Compressor Stabilization Techniques," ASME Turbo Expo 2003, Atlanta, Georgia, GT2003–38524.

Section II

Sensitivity Analysis Enhancements and Results with the U^2NCLE Software

Sensitivity Derivatives

For aerodynamic sensitivity analysis, the state equation is a system of nonlinear partial differential equations (PDE) expressing the conservation of mass, momentum, and energy. Differentiation of this system of PDE (i.e., sensitivity analysis) can be performed at one of two levels. In the first method, termed the continuous or variational approach, the PDE are differentiated prior to discretization, either directly or by introducing Lagrange multipliers which are defined as a set of continuous linear equations adjoint to the governing PDE. Subsequently, these directly differentiated or adjoint equations are discretized and solved. In the second method, termed the discrete approach, the PDE are differentiated after discretization. The discrete approach may also be cast in either a direct or an adjoint formulation, and the reader is referred to Hou et al.[1] for a comprehensive presentation of both discrete formulations. For a more detailed discussion on the continuous approaches to aerodynamic design optimization the interested reader is directed, for example, to Refs. 2-4

In general, the objective function and constraints may be expressed as $F_j\left(\beta_k, \vec{X}, \vec{Q}\right)$. Here, $\vec{Q}$ is the disciplinary state vector that is produced from the CFS, $\vec{X}$ is the computational mesh over which the PDE are discretized, and β_k the vector of design variables. The sensitivity derivatives of these functions, ∇F_j, may be expressed as

$$\nabla F_j = \frac{\partial F_j}{\partial \beta_k} + \left(\frac{\partial F_j}{\partial \vec{X}}\right)\frac{\partial \vec{X}}{\partial \beta_k} + \left(\frac{\partial F_j}{\partial \vec{Q}}\right)\frac{\partial \vec{Q}}{\partial \beta_k} \qquad j = 1,\ NCON+1 \tag{1}$$

To compute the sensitivity derivatives in Eq.(1), the sensitivity of the state vector, $\partial \vec{Q}/\partial \beta_k$, and the grid sensitivity terms, $\partial \vec{X}/\partial \beta_k$, are needed. This approach to sensitivity analysis is referred to as the direct differentiation method. The number of linear systems needing to be solved is equal to the number of design or independent variables, *NDV*. If in the design problem under consideration, the sum of the objective function and constraints is less than the number of design variables (i.e., *NCON+1 < NDV*), a more efficient alternative approach may be formulated. This method is referred to as the adjoint variable approach, and may be written as

$$\nabla F_j = \frac{\partial F_j}{\partial \beta_k} + \left(\frac{\partial F_j}{\partial \vec{X}}\right)\frac{\partial \vec{X}}{\partial \beta_k} - \vec{\lambda}^T_{F_j}\left[\frac{\partial \vec{R}}{\partial \beta_k} + \frac{\partial \vec{R}}{\partial \vec{X}}\frac{\partial \vec{X}}{\partial \beta_k}\right] \qquad j = 1,\ NCON+1 \tag{2}$$

where $\vec{R}$ represents the disciplinary state equation, and $\vec{\lambda}_{F_j}$ are adjoint vectors defined in such a way as to eliminate the dependence of the objective function and constraints on the sensitivity of the state vector. This method requires the solution of *NCON+1* linear systems. Hence, when the optimization problem formulation results in *NDV > NCON+1*, the adjoint variable approach should be used, whereas *NDV < NCON+1* the direct approach. Methods used to perform the sensitivity analysis are discussed in subsequent sections.

Discrete (Semi-Analytic) Approaches

For the discrete-direct approach (Eq.1), the sensitivity of the field variables are required, and for the discrete-adjoint approach (Eq. 2) the adjoint vectors are needed. To obtain these, the discrete residual vector for a steady-state solution may be recast as

$$\vec{R}\left(\beta_k, \vec{X}(\beta_k), \vec{Q}(\beta_k)\right) = 0 \tag{3}$$

where the explicit and implicit dependencies of the residual on the state vector $\vec{Q}(\beta_k)$, the computational mesh $\vec{X}(\beta_k)$, and the design variables β_k are asserted.

In the discrete-direct approach, Eq.(3) is directly differentiated with respect to the design variables to produce the following linear equation

$$\frac{d\vec{R}}{d\beta_k} = \frac{\partial \vec{R}}{\partial \beta_k} + \frac{\partial \vec{R}}{\partial \vec{X}} \frac{\partial \vec{X}}{\partial \beta_k} + \frac{\partial \vec{R}}{\partial \vec{Q}} \frac{\partial \vec{Q}}{\partial \beta_k} = 0 \tag{4a}$$

or, rearranging

$$\frac{\partial \vec{R}}{\partial \vec{Q}} \frac{\partial \vec{Q}}{\partial \beta_k} = -\left[\frac{\partial \vec{R}}{\partial \beta_k} + \frac{\partial \vec{R}}{\partial \vec{X}} \frac{\partial \vec{X}}{\partial \beta_k} \right] \tag{4b}$$

where $\partial\vec{R}/\partial\vec{Q}$ and $\partial\vec{R}/\partial\vec{X}$ are the Jacobian matrices evaluated with a converged (steady-state) solution. The solution of Eq.(4b) poses the difficulty of solving a large linear system of equations for each design variable. Furthermore, due to the fact that this is a linear system, the linearizations of the residual with respect to the state vector and the grid (i.e., the Jacobian matrices) must be exact. The detriments of using inexact linearizations in Eq.(4b) have been explored in Ref. 5. Solving these systems, however, is made more tractable when the above equations are recast into what has been termed the incremental iterative form [6,7] as follows

$$\tilde{A}\,\Delta^n\left(\frac{\partial \vec{Q}}{\partial \beta_k}\right) = -\left[\frac{\partial \vec{R}}{\partial \beta_k} + \frac{\partial \vec{R}}{\partial \vec{X}} \frac{\partial \vec{X}}{\partial \beta_k} + \frac{\partial \vec{R}}{\partial \vec{Q}} \frac{\partial \vec{Q}}{\partial \beta_k} \right] \tag{5a}$$

$$\left(\frac{\partial \vec{Q}}{\partial \beta_k}\right)^{n+1} = \left(\frac{\partial \vec{Q}}{\partial \beta_k}\right)^{n} + \Delta^n\left(\frac{\partial \vec{Q}}{\partial \beta_k}\right) \tag{5b}$$

where $\tilde{A}$ may be any convenient approximation to the higher-order Jacobian which converges the linear system. This is because the equations are now cast in delta form, with the physics contained in the right-hand-side vector. It has been found that the first-order Jacobian works well for use in the coefficient matrix of Eq.(5a); most CFS codes also use the first-order Jacobian for this purpose.

Two particularly attractive features of the incremental iterative strategy are that (*i*) a more diagonally dominant matrix may be used to drive the solution of the linear systems (as opposed to the sometimes ill-conditioned higher-order Jacobian), and (*ii*) the higher-order Jacobian now resides on the right-hand-side of the equations and may be dealt with in an explicit manner. When in this form, only the *k*-vectors resulting from the matrix-vector product of $(\partial\vec{R}/\partial\vec{Q})(\partial\vec{Q}/\partial\beta_k)$ are of concern. Hence, CPU time and memory efficient methods for constructing the exact matrix-vector product can be utilized. To this end, higher-order spatially accurate discrete-direct sensitivity analysis procedures have been developed and reported in Ref. 8.

The discrete-adjoint variable formulation begins by combining Eq.(4a) from the direct differentiation method with the sensitivity derivatives in Eq.(1). From this, adjoint vectors may be conveniently defined such that the sensitivity of the field variables are no longer needed. Omitting details, the end result requires the solution of the following linear systems for the adjoint vectors

$$\left(\frac{\partial \vec{R}}{\partial \vec{Q}}\right)^T \vec{\lambda}_{F_j} = \left(\frac{\partial F_j}{\partial \vec{Q}}\right)^T \qquad j = 1,\ NCON + 1 \tag{6}$$

The adjoint variable approach may also be recast in incremental iterative form, however, for brevity these details shall be omitted. It should be noted that all the same linearizations required by the direct approach are required by the adjoint variable method; they are simply transposed and used at different

stages in the computation of the sensitivity derivatives. Hence, a sensitivity analysis code which was developed for either of the discrete approaches may be modified to produce the other.

Numerical Approaches

The task of constructing exactly or analytically all of the required linearizations and derivatives by hand for either the discrete-direct or discrete-adjoint approach and then building the software for evaluating these terms can be extremely tedious. This problem is compounded by the inclusion of even the most elementary turbulence model (for viscous flow) or the use of a sophisticated grid generation package for adapting (or regenerating) the computational mesh to the latest design. One solution to this problem has been found in the use of a technique known as automatic differentiation. Application of this technique to an existing source code, that evaluates output functions, automatically generates another source code that evaluates both output functions and derivatives of those functions with respect to specified code input or internal parameters. A pre-compiler software tool, called ADIFOR (Automatic Differentiation of FORtran, Bischof et al.[9]), has been developed and utilized with much success to obtain complicated derivatives from advanced CFD and grid generation codes [10,11]. The use of ADIFOR produces code that, when executed, evaluates these derivatives of the output functions via a discrete-direct approach, referred to as forward-mode automatic differentiation. More recently, automatic differentiation software has emerged that enables the derivatives to be evaluated with a discrete-adjoint approach [12,13]. This type of automatic differentiation is known as reverse-mode. A detailed and concise review on the use of sensitivity analysis in aerodynamic shape optimization has been reported by Newman et al.[14], the reader is directed to this source for a discussion on the methods presented above.

The methods discussed above require differentiation of the CFS software, either by hand or with pre-compiler software. Other methods to obtain sensitivity derivatives are based on numerical techniques. The simplest numerical technique is the finite-difference approximation. Another is a new numerical technique, pioneered at MSU [15] for performing disciplinary and multidisciplinary sensitivity analysis which uses complex variables to approximate derivatives of real functions. This method is based on ideas that where explored over three decades ago by Lyness and Moler[16] and Lyness[17], and recently revisited by Squire and Trapp[18]. Both numerical approaches will be discussed below.

For a central finite-difference approximation to the derivative, one may expand the function in a Taylor series about a given point using a forward and a backward step, and then subtracting to yield

$$\frac{dF}{dx} = \frac{[F(x+h) - F(x-h)]}{2h} - \frac{h^2}{3!}\frac{d^3F}{dx^3} - \frac{h^4}{5!}\frac{d^5F}{dx^5} - \cdots \tag{7}$$

This expression for the derivative has a truncation error of $\mathcal{O}(h^2)$. The advantage of the finite-difference approximation to obtain sensitivity derivatives is that any existing code may be used without modification. The disadvantages of this method are the computational time required and the possible inaccuracy of the derivatives. The former is due to the fact that for every derivative, two well-converged CFS solutions for the function evaluations are required (i.e., 2**NDV* analyses). In the case of nonlinear fluid flow, for example, these solutions may become extremely expensive. The latter disadvantage is attributed to the sensitivity of the derivatives brought about by the choice of step size. To minimize the truncation error one selects a smaller step size, however, an exceedingly small step size may produce significant subtractive cancellation errors. The optimal choice for the step size is not known a priori, and may vary from one function to another, and from one design variable to the next.

Instead, if the function is expanded in a Taylor series using a complex step as

$$F(x+h\hat{i}) = F(x) + h\hat{i}\frac{dF}{dx} - \frac{h^2}{2!}\frac{d^2F}{dx^2} - \frac{h^3\hat{i}}{3!}\frac{d^3F}{dx^3} + \frac{h^4}{4!}\frac{d^4F}{dx^4} + \cdots \tag{8a}$$

Solving this expression for the imaginary part of the function yields

$$\frac{dF}{dx} = \frac{Im[F(x+h\hat{i})]}{h} + \frac{h^2}{3!}\frac{d^3F}{dx^3} - \frac{h^4}{5!}\frac{d^5F}{dx^5} + \cdots \tag{8b}$$

This expression for the derivative also has a truncation error of $\vartheta(h^2)$. By evaluating the function with a complex argument, both the function and its derivative are obtained, without subtractive terms, and thus cancellation errors are avoided. The real part is the function value to second order. This technique has been labeled as the complex Taylor series expansion (CTSE) method [15].

Previously, a disadvantage of the complex variable approximation was the increased runtime required by the evaluating routines when run with complex arguments. With current compiler options, and when the entire CFS code was converted to complex, that run time was on the order of three times the cost of the original solver. Automatic differentiated versions of analysis software, using say ADIFOR, incur about the same time penalties. Currently, the run time using the complex variable approximation costs little more than hand differentiated, direct-discrete approaches. A detailed comparison of sensitivity derivatives from automatic differentiated software and using the complex variable technique can be found in Ref. 19. The reader is directed to this source for a more complete discussion on the competing methods.

The advantages of the complex variable approximation for obtaining the derivatives are numerous. First, like the finite-difference approximation to the derivatives, very little modification to the software is required. All the original features and capabilities of the software are retained. Thus, user experience with the current software is not lost, and ongoing advancements and enhancements can be readily introduced into subsequent versions without extensive modifications or re-differentiation. This is in direct contrast to hand or automatically differentiated codes where any modification to the original software will require re-differentiation. This advantage is extremely useful in the problem formulation stages of the design process when new objective functions and constraints are being explored. Second, this method has been shown in Ref. 20 to be equivalent to a discrete-direct approach, either from automatic differentiation or hand differentiated codes solved in incremental iterative form, in the way that the state vector and its derivatives are being solved for simultaneously. When solving the state equation, the state vector resides in the real part and the derivatives in the imaginary part. Hence, fully converged flow solutions are not required to obtain derivatives of sufficient accuracy for design. Finally, the complex variable approximation to the derivative is not sensitive to the step size selection and only requires step sizes that avoid excessive truncation error; thus, this method demonstrates true second-order accuracy [15,21]. The CTSE method may also be used to construct any linearization or Jacobian required for CFS [22]. This may be particularly useful when complicated flux functions or turbulence models are being developed. In addition, the complex variable technique can be used to compute second derivative information using available data [19]; however, these computations are subject to cancellation errors.

Sensitivity Derivative Validation Study

In this section, validation of sensitivity derivative calculations for a three-dimensional wing are presented. Sensitivity derivatives with respect to lift and drag coefficients are computed with both the discrete-direct and discrete-adjoint formulations for low- and high-Reynolds number viscous, laminar flows. The configuration chosen is the standard benchmark ONERA M6 [23] wing, and the flow

conditions assumed are a Mach number of 0.52 with a 2.0° angle-of-attack. The y-coordinate of a grid point on the wing surface is selected as the independent variable.

In order to validate the computed sensitivity derivatives with finite-difference values, a detailed step-size study must first be performed using finite-differences. This is required in order to find an acceptable step-size for finite-differences, which are subjected to both truncation and cancellation errors. This study for sensitivity of lift and drag coefficients, at Reynolds numbers of 100 and $5 \cdot 10^6$, for forward, backward, and central finite differences are shown in Fig. 1. Step-sizes above and below that shown are subjected to the aforementioned errors, and can not be presented on the scale chosen in these plots. Selecting a finite-difference step-size of 10^{-8} to compare with, the computed sensitivity of lift and drag for the low- and high-Reynolds number simulations are given in Table 1 and Table 2, respectively. Observe that the accuracy of the computed derivatives, using both the direct and adjoint formulations, agree to within 1% of the central finite-difference value. Although this accuracy is exceptional, it is more than that which is required to perform computational design, error estimation, or uncertainty analysis. Note, however, that obtaining accurate sensitivity derivatives using finite-differences is usually difficult, if not impossible. Hence, standard test configurations such as the ONERA M6, which have been used for code validation and numerous sensitivity analysis studies, are a prerequisite.

The direct approach to sensitivity analysis produces the derivative of state vector with respect to the independent variable. Hence, it physically represents the rate of change of dependent to independent variable. The adjoint vector, on the other had, does not have an obvious physical interpretation, but it does represent the rate of change in the objective/constraint function (see Eq. 6) to the state-equation. Thus, the adjoint vector has utility in error estimation, error correction, and grid adaptation. The use of the adjoint vector for this purpose has been explored in Ref. 24.

Conclusion

In the current research, both the discrete-direct and the discrete-adjoint formulations for sensitivity analysis have been incorporated into the U^2NCLE software and validated for compressible viscous, laminar flows on a benchmark configuration. This validation study included a detailed finite-difference step-size study in order to compare with accurate numerical derivatives. It should be noted that for rotating machinery the rotational speed, and therefore the dynamic grid terms, are not a function of the geometric shape of the configuration. Hence, the linearizations for the discrete sensitivity analysis performed in this study are valid for that type of analysis as well.

References

1. Hou, G.J.-W., Taylor III, A.C., and Korivi, V.M., "Discrete Shape Sensitivity Equations for Aerodynamic Problems," *Int. J. Num. Meth. Engr.*, Vol. 37, 1994, pp. 2251-2266.
2. Jameson, A., "Aerodynamic Design via Control Theory," *J. Sci. Comp.*, Vol. 3, 1988, pp. 233-260.
3. Anderson, W.K., and Venkatakrishnan, V., "Aerodynamic Design Optimization on Unstructured Grids with a Continuous Adjoint Formulation," AIAA Paper No. 97-0643, Jan. 1997.
4. Iollo, A., Salas, M., and Ta'asan, S., "Shape Optimization Governed by the Euler Equations Using an Adjoint Method," ICASE Report No. 93-78, Nov. 1993.
5. Newman III, J.C., Taylor III, A.C., and Burgreen, G.W., "An Unstructured Grid Approach to Sensitivity Analysis and Shape Optimization Using the Euler Equations," AIAA Paper No. 95-1646, June 1995.
6. Korivi, V.M., Taylor III, A.C., Newman, P.A., Hou, G.J.-W., and Jones, H.E., "An Approximately Factored Incremental Strategy for Calculating Consistent Discrete CFD Sensitivity Derivatives," *J. Comp. Physics*, Vol. 113, No. 2, 1994, pp. 336-346.
7. Sherman, L.L., Taylor III, A.C., Green, L.L., Newman, P.A., Hou, G.J.-W., and Korivi, V.M., "First- and Second-Order Aerodynamic Sensitivity Derivatives via Automatic Differentiation with Incremental Iterative Methods," *J. Comp. Physics*, Vol. 129, No. 2, 1996, pp. 307-336.

8. Newman III, J.C., Taylor III, A.C., and Barnwell, R.W., "Aerodynamic Shape Sensitivity Analysis and Design Optimization of Complex Configurations Using Unstructured Grids," *Bound Proc., 15th AIAA Applied Aerodynamics Conf.*, AIAA Paper No. 97-2275, June 1997.
9. Bischof, C., and Griewank, A., "ADIFOR: A Fortran System for Portable Automatic Differentiation," AIAA Paper No. 92-4744, Sept. 1992.
10. Green, L.L., Newman, P.A., and Haigler, K.J., "Sensitivity Derivatives for Advanced CFD Algorithms and Viscous Modeling Parameters Via Automatic Differentiation," *J. Comp. Physics*, Vol. 125, 1996, pp. 313-324.
11. Taylor III, A.C., Oloso, A., and Newman III, J.C., "CFL3D.ADII (Version 2.0): An Efficient, Accurate, General-Purpose Code for Flow Shape-Sensitivity Analysis," *Bound Proc., 15th AIAA Applied Aerodynamics Conf.*, AIAA Paper No. 97-2204, June 1997.
12. Mohammadi, B, "Optimal Shape Design, Reverse Mode of Automatic Differentiation and Turbulence," AIAA Paper No. 97-0099, Jan. 1997.
13. Carle, A., Fagan, M., and Green, L.L, "Preliminary Results From the Application of Automated Adjoint Code Generation to CFL3D," AIAA Paper No. 98-4807, Sept. 1998.
14. Newman III, J.C., Taylor III, A.C., Barnwell, R.W., Newman, P.A., and Hou, G.J.-W., "Overview of Sensitivity Analysis and Shape Optimization for Complex Aerodynamic Configurations," *J. of Aircraft*, Vol. 36, No. 1, Jan. 1999, pp. 87-96
15. Newman III, J.C., Anderson, W.K., and Whitfield, D.L., "Multidisciplinary Sensitivity Derivatives Using Complex Variables," Mississippi State University Report MSSU-EIRS-ERC-98-08, July 1998.
16. Lyness, J.N., and Moler, C.B., "Numerical Differentiation of Analytic Functions," *SIAM J. Numer. Anal.*, Vol. 4, 1967, pp. 202-210.
17. Lyness, J.N., "Numerical Algorithms Based on the Theory of Complex Variables," *Proc. ACM 22nd Nat. Conf.*, Thomas Book Co., Washington, DC, 1967, pp. 124-134.
18. Squire, W., and Trapp, G., "Using Complex Variables to Estimate Derivatives of Real Functions," *SIAM Rev.*, Vol. 10, No. 1, March 1998, pp. 110-112.
19. Anderson, W.K., Newman III, J.C., Whitfield, D.L., and Nielsen, E.J., "Sensitivity Analysis for the Navier-Stokes Equations on Unstructured Meshes," *AIAA J.*, Vol. 39, No. 1, Jan. 2001, pp. 56-63.
20. Burg, C.O.E., and Newman III, J.C., "Efficient Numerical Design Optimization Using Highly Accurate Derivatives via the Complex Taylor's Series Expansion Method," *J. of Computers and Fluids*, accepted- to appear.
21. Newman III, J.C., Whitfield, D.L., and Anderson, W.K., "A Step-Size Independent Approach for Multidisciplinary Sensitivity Analysis and Design Optimization," *Bound Proc., 17th AIAA Applied Aerodynamics Conf.*, AIAA Paper No. 99-3101, June 1999.
22. Whitfield, D.L., and Taylor, L.K., "Variants of a Two-Level Method for the Approximate Numerical Solution of Field Simulation Equations," Mississippi State University Report MSSU-COE-ERC 98-09, July 1998.
23. Schmitt, V., and Charpin, F., "Pressure Distributions on the ONERA M6 Wing at Transonic Mach Numbers," AGARD Report No. 138, May 1979.
24. Balasubramanian, R., and Newman III, J.C., "Error Estimation and Grid Adaptation for Functional Outputs Using Discrete-Adjoint Sensitivity Analysis," *Computers and Fluids*, under review.

FIGURES

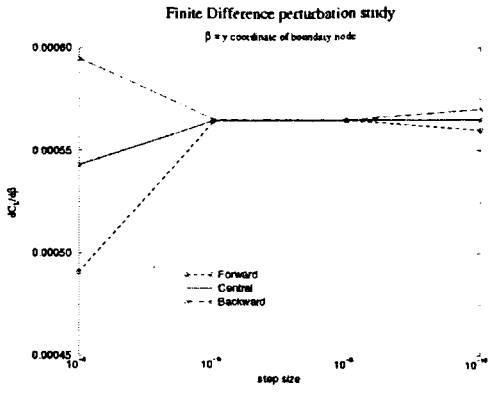

(a) Sensitivity of lift, Re=100.

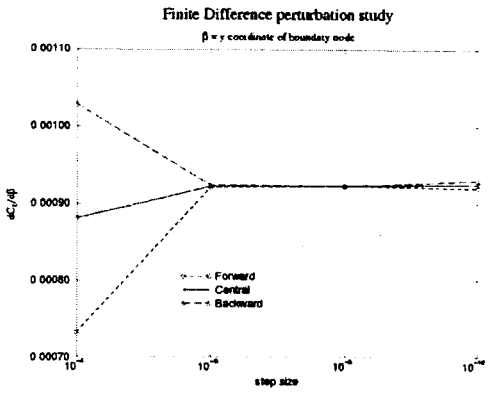

(b) Sensitivity of drag, Re=100.

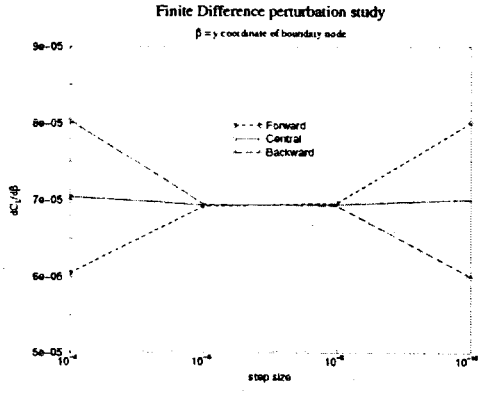

(c) Sensitivity of lift, Re=$5 \cdot 10^6$.

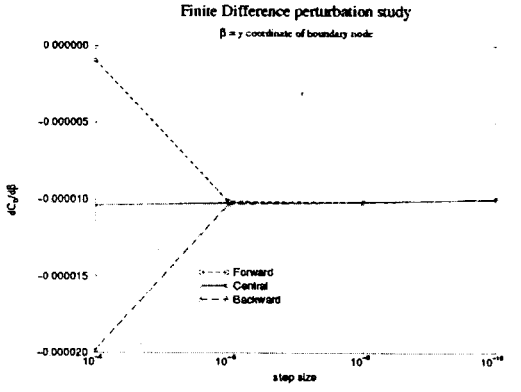

(d) Sensitivity of drag, Re=$5 \cdot 10^6$.

Figure 1: Step-size study for finite-difference sensitivity derivatives.

Table 1: Comparison of sensitivity derivatives, Reynolds number of 100.

Sensitivity	Direct Analysis	Adjoint Analysis	Finite Difference*
$dC_L/d\beta$	0.000565	0.000565	0.000565
$dC_D/d\beta$	0.000927	0.000926	0.000922

* Central finite difference for step size of 10^{-8}

Table 2: Comparison of sensitivity derivatives, Reynolds number of $5 \cdot 10^6$.

Sensitivity	Direct Analysis	Adjoint Analysis	Finite Difference*
$dC_L/d\beta$	0.0000691	0.0000697	0.0000693
$dC_D/d\beta$	-0.0000102	-0.0000102	-0.0000102

* Central finite difference for step size of 10^{-8}